Structural Engineering and Mechanics, Vol. 21, No. 6 (2005) 737-765

DOI: http://dx.doi.org/10.12989/sem.2005.21.6.737

Partially confined circular members subjected to axial compression: Analysis of concrete confined by steel ties

R. Eid†

Department of Civil Engineering, University of Sherbrooke, Sherbrooke, Quebec, Canada J1J 2R1

A. N. Dancygier‡

National Building Research Institute, Department of Structural Engineering and Construction Management, Faculty of Civil and Environmental Engineering, Technion-Israel Institute of Technology, Technion City, Haifa 32000, Israel

(Received August 2, 2004, Accepted October 5, 2005)

Abstract. This paper presents a theoretical model for the behavior of partially confined axi-symmetric reinforced concrete members subjected to axial load. The analysis uses the theories of elasticity and plasticity to cover the full range of the concrete behavior. Analysis of the elastic range of the problem involves boundary conditions that are defined along a relatively simple geometry. However, extending the analysis into the plastic range involves difficulties that arise from the irregular geometry of the boundary between the plastic zone and the elastic zone, a boundary which is also changing as the axial load increases. The solution is derived by replacing the discrete steel ties with an equivalent tube of thickness t_{eq} and by analyzing the concrete cylinder, which is uniformly confined by the equivalent tube. The equivalency criterion initiates from a theoretical analysis of the problem in its elastic range where further finite element analysis shows that this criterion is valid also for the plastic range of the cylinder material. According to the proposed model, the efficiency of the lateral reinforcement can be evaluated by the equivalent thickness t_{eq}. Comparison with published test results of confined reinforced concrete stress-strain curves shows good agreement between the test and the analytical results.

Key words: confined concrete; steel ties; plasticity.

1. Introduction

1.1 Models of concrete confined by lateral ties

Early studies of confined concrete have shown that hydrostatic pressure (active pressure) on concrete cylinders increases concrete strength and ductility (Richart *et al.* 1928). During the last three decades, research has examined the effect of passive confinement due to lateral and longitudinal reinforcement. Based on extensive study, researchers (e.g., Mander *et al.* 1984, Scott *et al.* 1982, Sheikh and Uzumeri 1980) arrived at a number of conclusions regarding the importance of

† Postdoctoral Fellow
‡ Senior Lecturer, Corresponding author, E-mail: cvravid@techunix.technion.ac.il

concrete confinement, provided by the reinforcement. They found that in order to enhance the behavior of RC structural elements under compression, lateral reinforcement should be placed at relatively close spacing, the longitudinal reinforcement should be well distributed around the cross-section perimeter and the yield strength of the lateral reinforcement should be increased. They also found that spirals or circular hoops are more efficient than rectangular hoops.

Research and modeling of concrete confined by lateral reinforcement (i.e., stirrups or ties) can be classified into four main approaches (or stages). The first approach is empirical, in which the stress-strain relationship of confined concrete were fitted to experimental results (Park *et al.* 1982, Fafitis and Shah 1985, Hoshikuma *et al.* 1997). Another approach is based on a physical-engineering model that deduces an arch action between the lateral reinforcement ties (or stirrups). This arch action, which is presumed to be parabolic, provides the lateral pressure that causes the confined behavior of the concrete core (Sheikh and Uzumeri 1982). Therefore, the "effectively confined core area" (ECCA), has a parabolic shape in the vertical and horizontal directions. The parabolic shape and the initial slope of the parabola (45°) were derived from experimental results (Sheikh and Uzumeri 1980). Further study was done by Mander *et al.* (1988) using the ECCA concept to develop a unified stress-strain model for confined concrete with a monotonic and cyclic loading, based on an equation proposed by Popovics (1973). The models that are based on the physical-engineering approach assume that the lateral steel yields before the concrete reaches its confined strength. The third approach is based either on the first or on the second approach, however, rather than assuming yielding of the confining steel it includes computation of the steel stress (at the concrete peak stress) either by introducing compatibility conditions (at the concrete-tie interface) or by introducing empirical expressions (Saatcioglu and Razvi 1999). The compatibility conditions are solved by an iterative procedure (Cusson and Paultre 1995) or by a direct formulation (Legeron and Paultre 2003). The fourth approach was introduced by Karabinis and Kiousis (1994), which proposed a plasticity model for the confined concrete core. The shape of the confined core, on which their model has been applied, was based on the assumption of the parabolic arch action (Sheikh and Uzumeri 1980, 1982).

This paper presents a theoretical model for concrete confined by steel ties. It analyzes the concrete behavior according to the theory of plasticity. However, instead of presuming a parabolic shape of the effectively confined concrete core the current model proposes a way to analyze an equivalent uniformly confined concrete cylinder. The equivalency criterion initiates from a theoretical analysis of the problem in its elastic range. Nevertheless, further finite element calculations show that this criterion is valid also in the non-linear range of the cylinder material and various experimentally measured stress-strain relationships that were calculated by the proposed model show good agreement with the experimental results.

1.2 Basis for the current model

The solution to the problem of a cylinder subjected to axial pressure and confined by the passive action of lateral elastic-perfectly plastic rings (see Fig. 1a) was presented by Eid (2004) and it is valid for the elastic behavior of the cylinder. The variables of the elastic problem are as follows (see also Fig. 1a):

a - cylinder's radius;
b & t - width and thickness of the confining rings;
s - clear spacing between the rings;
q - axial pressure (positive in compression);

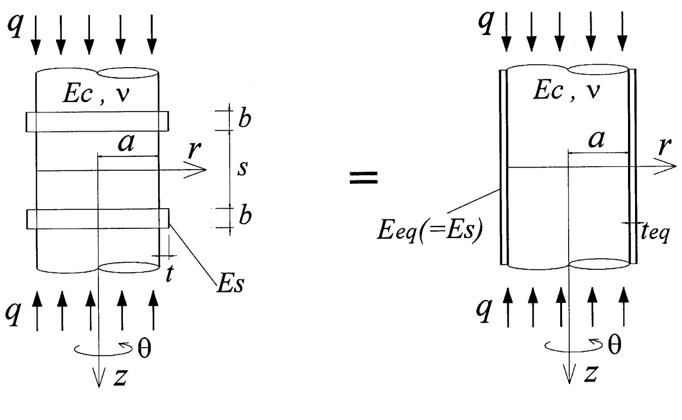

Fig. 1 Description of the problem: (a) Concrete cylinder confined by steel rings and (b) the equivalent cylinder

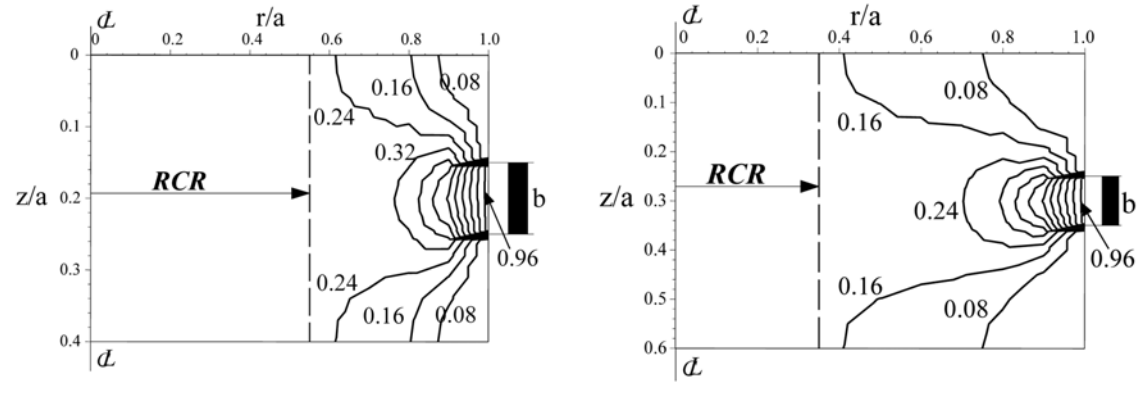

Fig. 2 Contour maps of radial stresses (normalized with respect to the rings' confining pressure p) for two cases of spacing: (a) $s_1 = 0.3$ and (b) $s_1 = 0.5$, in a cylinder, confined by rings with $b_1 = 0.1$ and $\nu = 0.2$

E_c, ν - Young's modulus and Poisson ratio of the cylinder;
E_s - Young's modulus of the confining rings;
m - confinement-to-cylinder modulus ratio, E_s/E_c;

Additionally, in order to obtain a more general solution, which pertains to "families of cases" these variables have been normalized into non-dimensional variables noted by an index "1" (e.g., $b_1 = b/a$, $s_1 = s/a$). The radius of the cylinder analyzed in this work (a) is equal to the radius of the concrete core that is confined inside the lateral reinforcement (ties), i.e., it does not include the concrete cover.

The elastic solution shows that within a reduced cylinder radius (*RCR*) there is a zone of uniformly distributed stresses, in which the tangential stress is equal to the radial stress and the axial and shear stresses are equal to zero (Eid 2004) as shown in Fig. 2. This behavior within the *RCR* is typical of a fully confined cylinder, which is acted along its surface by a uniform lateral pressure. Unlike the elastic problem, in which the boundary conditions are defined along a relatively simple geometry, developing this solution into the plastic range involves difficulties that arise from the irregular geometry of the boundary between the plastic zone and the elastic zone, a boundary which is also changing as the axial load increases.

This mathematical difficulty leads to the need of an approximate solution for this problem. Based on the concept of the *RCR*, the original problem can be represented by an equivalent model of a concrete cylinder confined by a uniform steel tube. As opposed to the original problem, the equivalent model has relatively simple boundary conditions, which make the problem simpler for analysis by elasto-plastic material models.

2. Equivalent uniform confinement model

2.1 The concept of equivalent uniform confinement

The concept of the *RCR* that was observed in the elastic solution (Eid 2004) can be applied for the full elasto-plastic analysis of an equivalent cylinder with uniform boundary conditions that are provided by a uniform equivalent tube of constant thickness t_{eq}, and modulus of elasticity E_{eq} which represents the ties (Fig. 1). The radius of the equivalent cylinder is taken as equal to that of the original problem in order to include the confinement effect near the cylinder surface, outside the elastically observed *RCR* (e.g., as in Fig. 2). Therefore, a proper criterion must be set for the properties of the equivalent uniform tube. It should be noted that with regards to the equivalency criterion the equivalent tube can be of any material (i.e., E_{eq} can be the modulus of elasticity of any material). However, in order to preserve the response of the steel ties (to the action of the axial pressure) during the elasto-plastic range of the analysis – the tube should respond in the same way as the ties that it represents, hence, it should have their mechanical properties (i.e., $E_{eq} = E_s$, Fig. 1). Thus, an equivalency criterion is required only for setting the thickness t_{eq} of the tube.

2.2 Equivalency criterion

Since the problem of a concrete column that is partially confined by steel ties is commonly characterized by the axial stress-strain relationship, the axial strain ε_z is chosen here for determining the equivalency criterion. This criterion initiates from the elastic analysis of a partially confined cylinder, as explained in the following text.

Consider the longitudinal (axial) strain of the partially confined cylinder due to the action of the confining rings (Fig. 1) ε_z^c, which is given by:

$$\varepsilon_z^c(r, z) = \frac{1}{E_c}[\sigma_z - \nu(\sigma_r + \sigma_\theta)] = \frac{p}{E_c}\int_0^\infty f_2 dk_1 \tag{1}$$

where p is a lateral pressure that is applied by the ring (assumed constant over its width). The function f_2 is obtained from substitution of the stresses σ_z, σ_r and σ_θ in Eq. (1), where the expressions of the stresses are given in Eid (2004). This substitution results in f_2, which is a function of the non-dimensional variables ν, β, r_1, z_1, s_1, b_1, and it is given by:

$$f_2 = \{[4(1-\nu^2)-(1+\nu)\beta]I_0(k_1r_1)+k_1r_1(1+\nu)I_1(k_1r_1)\}k_1^3f_1(k_1)\sin\left(\frac{k_1b_1}{2}\right)\cdot$$

$$\cdot\left[\sum_{i=1}^{n}\cos\frac{k_1}{2}(2i-1)(s_1+b_1)\right]\cos(k_1z_1) \tag{2}$$

where n is the number of pairs of rings applied symmetrically with respect to the origin and β and $f_1(k_1)$ are given by:

$$\beta = 2(1-\nu)+ka\frac{I_0(ka)}{I_1(ka)} \tag{3}$$

$$f_1(k_1) = -\frac{4}{\pi k_1^4}\left[\frac{1}{(1-2\nu-\beta)I_0(k_1)+(k_1+\beta/k_1)I_1(k_1)}\right] \tag{4}$$

where k is the wave number (a constant with a dimension of length^{-1}) and $k_1 = ka$. $I_0(\zeta)$ and $I_1(\zeta)$ are order zero and one modified Bessel functions (of the first kind) of the general argument ζ. The geometrical variables in Eqs. (1)-(4) are defined in Fig. 1, and subscript "1" denotes their normalization with respect to the radius a.

Fig. 3 shows the variation of the strain ε_z^c versus r/a (r_1) for $b_1 = 0.1$, $s_1 = 0.3$ (Fig. 3a) and for $s_1 = 0.5$ (Fig. 3b). It can be seen in the figure that the longitudinal strain ε_z^c obtained from the elastic solution is also constant within an *RCR* but varies significantly near the cylinder surface. Let $\varepsilon_{z,\,r-avg}^c$ be the axial strain averaged over the radius at a given *z due to the action of the rings*. It is further noted that when the axial strain is averaged over the full cylinder's radius (i.e., within $r = 0$ to a) it is very close to the constant ε_z^c within the *RCR* ($\varepsilon_{z,\,r-avg}^c$ at $z = 0$, Fig. 3).

Hence, the axial strain is averaged over the radius and along the longitudinal axis within a typical confined zone between two pressure bands (i.e., within the range $-(s+b)/2 < z < (s+b)/2$, Fig. 1)

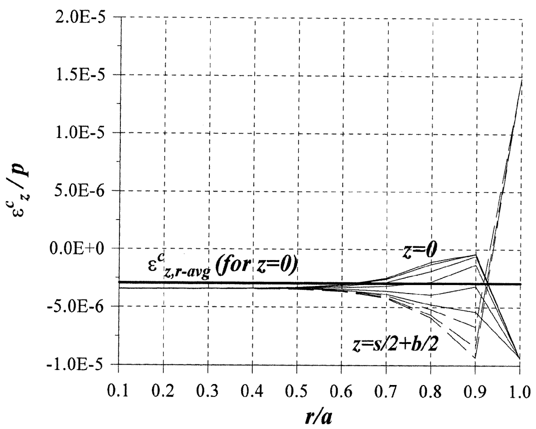

(a)

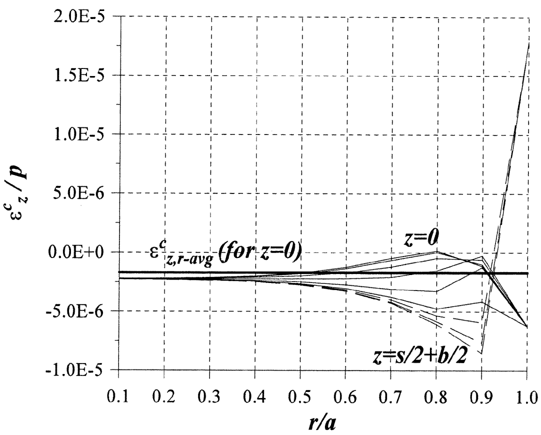

(b)

Fig. 3 Distribution of the axial strain due to the ring action for (a) $s_1 = 0.3$ and (b) $s_1 = 0.5$, in a cylinder, confined by rings with $b_1 = 0.1$, $t_1m = 0.35$ and $\nu = 0.2$, $E_c = 30000$ MPa (Note that compression is positive) and it is denoted here $\varepsilon^c_{z,avg}$. Thus, for the partially confined cylinder (due to the action of the confining rings), $\varepsilon^c_{z,avg}$, is given by:

$$\varepsilon^c_{z,avg} = \frac{2\pi \int_{-(s+b)/2}^{(s+b)/2} \int_0^a \varepsilon^c_z(r,z) r dr dz}{\pi a^2 (s+b)} = 2\frac{p}{E_c} \frac{\int_{-(s_1+b_1)/2}^{(s_1+b_1)/2} \int_0^1 \int_0^\infty f_2 dk_1 r_1 dr_1 dz_1}{(s_1+b_1)} \tag{5}$$

It should be noted that the *total* average axial strain $\varepsilon_{z,avg}$ is composed of the constant strain due to the action of the longitudinal (axial) stress acting at the ends of the column, q, and of the average axial strain of the partially confined cylinder due to the (elastic) action of the confining rings $\varepsilon^c_{z,avg}$ [given in Eq. (5)]. Thus, the *total* average axial strain $\varepsilon_{z,avg}$, is given by:

$$\varepsilon_{z,avg} = \frac{q}{E_c} + \varepsilon^c_{z,avg} \tag{6}$$

It can be shown that the axial strain $\varepsilon_{z,tu}$ in a cylinder that is fully confined by a tube of thickness t_{eq}, with a confinement-to-cylinder modulus ratio m, radius a and under an axial pressure q, is given by:

$$\varepsilon_{z,tu} = \frac{q}{E_c}\left[\frac{a + m(1+\nu)(1-2\nu)t_{eq}}{a + m(1-\nu)t_{eq}}\right] \tag{7}$$

The equivalent thickness t_{eq} is computed by equating the total average axial strain of the partially confined cylinder $\varepsilon_{z,avg}$ Eq. (6) to the axial strain of a fully confined equivalent cylinder (Eq. 7), as follows:

$$\underbrace{\frac{q}{E_c}\left[\frac{a + m(1+\nu)(1-2\nu)t_{eq}}{a + m(1-\nu)t_{eq}}\right]}_{\textit{equivalent cylinder (Eq. 7)}} = \underbrace{\varepsilon_{z,avg}}_{\substack{\textit{partially confined} \\ \textit{original cylinder (Eq. 6)}}} \tag{8}$$

Rearranging terms in Eq. (8) yields an expression for the equivalent thickness t_{eq}:

$$\frac{t_{eq}}{a} = \frac{\left(\frac{q}{E_c \varepsilon_{z,avg}} - 1\right)}{m\left[1 - \nu - \frac{q}{E_c \varepsilon_{z,avg}}(1+\nu)(1-2\nu)\right]} \tag{9}$$

2.2.1 Calculation of the average axial strain

It is noted that the expression $\varepsilon^c_{z,avg} \cdot (s_1 + b_1) \cdot a$ (see Eq. 5) is also equal to the difference between the averaged displacements of two cross-sections normal to the longitudinal (z) axis, located at a distance of a typical zone $\Delta z = s + b$ from each other. Hence, from Eq. (5) it follows that:

$$\varepsilon^c_{z,avg} \cdot (s_1 + b_1) \cdot a = 2a\frac{p}{E_c} \int_{-(s_1+b_1)/2}^{(s_1+b_1)/2} \int_0^1 \int_0^\infty f_2 dk_1 r_1 dr_1 dz_1 =$$

$$= \frac{1}{\pi a^2} \int_0^{2\pi} d\theta \int_0^a [w(z+s+b) - w(z)] r dr = 2\int_0^1 \Delta w_{\Delta z = s+b} r_1 dr_1 \tag{10}$$

where w is the axial displacement and $\Delta w_{\Delta z = s+b}$ is the difference between axial displacements at two points, located at a distance equal to that of a typical zone $\Delta z = s + b$.

The pressure acting on the cylinder's surface due to the action of the confining rings is repeated over a typical zone Δz. Therefore $\Delta w_{\Delta z = s+b}$ is constant and it depends neither on z nor on r. This deduction was confirmed by several examples with different problem's parameters. For example, Fig. 4 shows the axial displacements of several cross-sections for $b_1 = 0.1$, $s_1 = 1.0$, $p/E_c = 3.33 \cdot 10^{-6}$ and $\nu = 0.15$. It can be seen that $\Delta w_{\Delta z = s+b}$ remains constant for any radius r (or r_1) or for any axial coordinate z (provided that $\Delta z = s + b$).

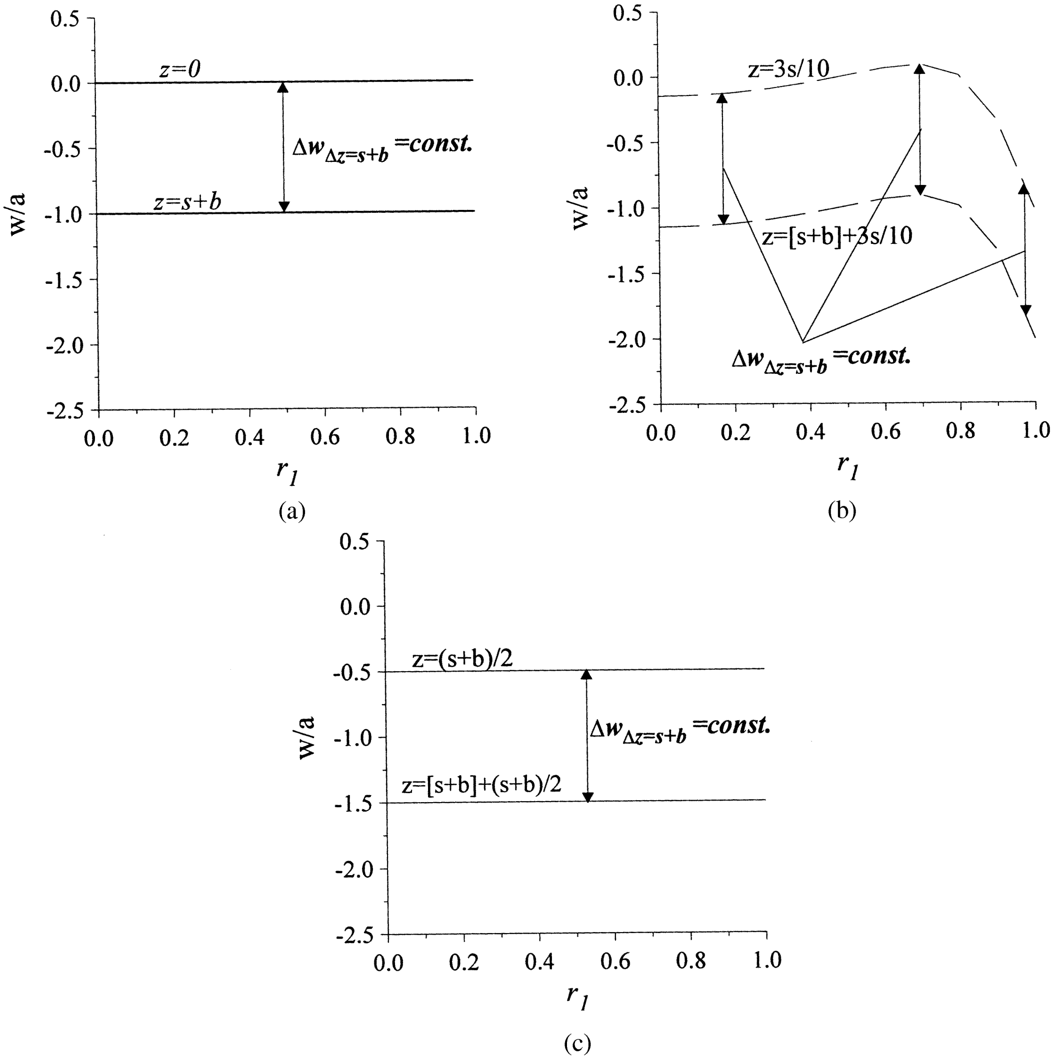

Fig. 4 Distribution of normalized axial displacements resulting from the lateral pressure of the confining rings along several cylinder's cross-sections for $b_1 = 0.1$, $s_1 = 1.0$, $p/E_c = 3.33 \cdot 10^{-6}$ and $\nu = 0.15$. Note that $\Delta w_{\Delta z = s+b}$ is equal for any two cross-sections that are $(s + b)$ apart

Introducing in Eq. (10) a constant $\Delta w_{\Delta z = s+b}$ yields the following expression:

$$\varepsilon_{z,\,avg}^{c} \cdot (s_1 + b_1) = \frac{1}{a}\Delta w_{\Delta z = s+b} = const. = 2\frac{p}{E_c}\int_{-(s_1+b_1)/2}^{(s_1+b_1)/2}\int_0^1\int_0^\infty f_2 dk_1 r_1 dr_1 dz_1 \tag{11}$$

Hence, for any given level of a lateral pressure p the following expression can be written:

$$F_2 = \int_{-(s_1+b_1)/2}^{(s_1+b_1)/2}\int_0^1\int_0^\infty f_2 dk_1 r_1 dr_1 dz_1 = const. \tag{12}$$

Furthermore, at the limit case of $s_1 = 0$ the average axial strain of the partially confined cylinder due to the confining rings $\varepsilon_{z,\,avg}^{c}$ is equal to the axial strain of the fully confined cylinder, which is given by:

$$\varepsilon_{z,\,avg}^{c}(s_1 = 0) = \varepsilon_z^c(uniform\ confinement) = -\frac{2p\nu}{E_c} \tag{13}$$

Substituting terms from Eqs. (12) and (13) into Eq. (11) yields the constant F_2 (Eq. 12) and $\varepsilon_{z,\,avg}^{c}$ as follows:

$$F_2 = -\nu b_1, \qquad \varepsilon_{z,\,avg}^{c} = 2\frac{p}{E_c}\frac{-\nu b_1}{(s_1 + b_1)} \tag{14}$$

The following expression for the *total* average strain $\varepsilon_{z,\,avg}$ is obtained from substituting $\varepsilon_{z,\,avg}^{c}$ from Eq. (14) into Eq. (6):

$$\varepsilon_{z,\,avg} = \frac{q}{E_c} + \frac{p}{E_c}\frac{-2\nu b_1}{(s_1 + b_1)} = \frac{q}{E_c}\left(1 - 2f_3\frac{\nu b_1}{(s_1 + b_1)}\right) \tag{15}$$

where f_3 is the p/q ratio, which is given by Eid (2004):

$$f_3 = \frac{p}{q} = \frac{\nu}{\dfrac{8(1-\nu^2)}{\pi}\displaystyle\int_0^\infty \frac{\sin\left(\dfrac{k_1 b_1}{2}\right)\left[\displaystyle\sum_{i=1}^{n}\cos\frac{k_1}{2}(2i-1)(s_1+b_1)\right]\cos\left[\dfrac{k_1}{2}(s_1+b_1)\right]}{k_1^3\dfrac{I_0(k_1)^2}{I_1(k_1)^2} + (2\nu - k_1^2 - 2)k_1}dk_1 + \dfrac{1}{t_1 m}} \tag{16}$$

The summation in Eq. (16) represents the accumulative influence of the confining rings (ties). It can be shown (Eid 2004) that f_3 converges for five pairs of rings ($n = 5$ in Eq. 16).

Substituting $\varepsilon_{z,\,avg}$ from Eq. (15) into Eq. (9) and rearranging terms yields the following expression for the equivalent confining tube thickness normalized with respect to the cylinder's radius, a:

$$t_{eq1} = \frac{t_{eq}}{a} = \frac{f_3}{m\left[(\nu - 1)f_3 + \nu\left(\dfrac{s_1}{b_1} + 1\right)\right]} \tag{17}$$

Eqs. (16) and (17) show that t_{eq} depends on the geometrical parameters a, s_1, b_1, on the concrete Poisson's ratio ν, on the modulii ratio m and on the mixed geometrical-mechanical parameter $t_1 m$.

According to these parameters of the problem, the full elasto-plastic analysis of the original partially confined cylinder can be replaced by an analysis of an equivalent cylinder, confined inside a uniform tube whose thickness is given by Eq. (17). The mechanical properties of the materials in the original and in the equivalent problems remain the same.

3. Elasto-plastic analysis of the equivalent model

Once the parameters of the equivalent confined cylinder are determined it can be analyzed with proper material models for the confined concrete and for the confining equivalent tube.

3.1 The concrete constitutive model

Several relatively recent models that are based on the theory of plasticity have been proposed to simulate the tri-axial behavior of concrete (e.g., Karabinis and Kiousis 1994, Imran and Pantazopoulou 2001, Grassl *et al.* 2002). The Imran and Pantazopoulou (2001) concrete plasticity model was developed using experimental background of 130 tri-axial tests conducted on cylindrical specimens. This model is applied herein to represent the compression behavior of the concrete confined in the equivalent tube (and hence of concrete confined by lateral steel rings). The main features of this plasticity model are given in Appendix I.

It should be noted though, that the original model was developed for the case of a known (active) constant lateral pressure that acts on the concrete to provide the confinement. Thus, the model includes a constant parameter that represents the maximum (contraction) volumetric strain $\varepsilon_{v,\max}$, which is determined empirically (Imran and Pantazopoulou 2001). In the case of concrete confined by lateral reinforcement, the lateral steel responds to the axial pressure and hence, the lateral (passive) pressure is developed with the axial pressure or strain (and according to the steel constitutive model). As a result the parameter that represents the maximum (contraction) volumetric strain increases with the increase of the lateral pressure. A constant value of $\varepsilon_{v,\max}$ is not suitable for this case and therefore, the concrete constitutive model of Imran and Pantazopoulou (2001) is applied here with an expression for a variable maximum volumetric strain. This expression is derived from a function of ε_v (see Eq. (A.7) in Appendix I), which was also proposed by these researchers (Imran and Pantazopoulou 1996).

3.2 The steel constitutive relations

The steel behavior, described in Fig. 5, is uniaxial because the bars and ties are loaded uniaxially. Depending on the type of the steel and for most cases, an elastic-perfectly plastic curve can be used (denoted as *EPP* in Fig. 5). Elastic-plastic steel behavior that includes hardening is represented by a stress-strain curve denoted EPH in Fig. 5. The steel hardening initiates at a strain denoted ε_{sh} (Fig. 5) and it is modeled by a multi-linear curve. Additionally, the constitutive relations of reinforcing steel that has rounded stress-strain curves are modeled by a multi-linear curve denoted ML in Fig. 5.

The quantitative parameters (e.g., ε_{sh}, ε_{su}, f_y, in Fig. 5) are set according to the reported properties of the reinforcing steel.

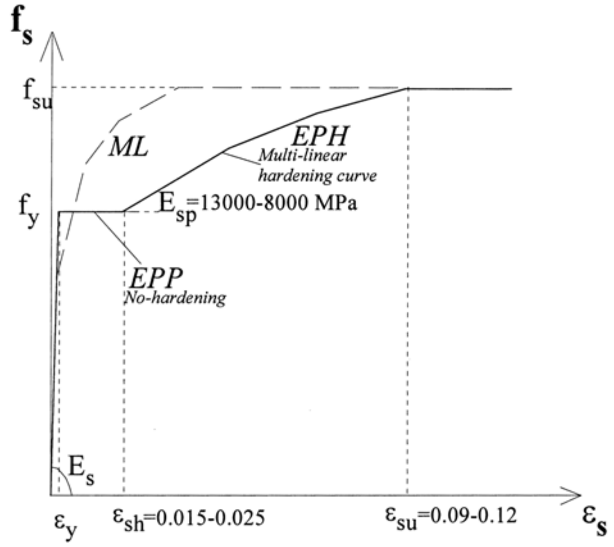

Fig. 5 Constitutive relations of the reinforcing steel

3.3 The solution procedure

The stress-strain curve of an axially loaded concrete column confined by steel ties is obtained by analyzing its equivalent uniformly confined cylinder whose axial strain ε_z is increased incrementally. First, determine the equivalent model's parameters, which are as follows:

- The concrete's core diameter;
- The concrete material constants (according to Table 1 in Imran and Pantazopoulou 2001);
- The steel material constants (see Fig. 5);
- The thickness of the equivalent circumferential steel tube t_{eq} Eq. (17)

Initially the model's response is elastic [with suitable elastic constants that correspond to the concrete strength, e.g., $E_c = 5000\sqrt{f_{c0}}$ (Mander *et al.* 1988), where f_{c0} and E_c are given in MPa and $\nu = 0.15$]. Once Eq. (A.1) (see Appendix I) is satisfied the material's behavior goes into the elasto-plastic range. In this range the incremental stress tensor is calculated according to the elastic incremental strain tensor, as follows:

$$d\sigma_{ij} = C_{ijkl} d\varepsilon_{kl}^{e} = C_{ijkl}(d\varepsilon_{kl} - d\varepsilon_{kl}^{p}) \quad (18)$$

where, C_{ijkl} is the isotropic material tensor and $d\varepsilon_{kl}^{p}$ is the plastic incremental strain tensor.

Using the consistency condition $df = 0$, which requires that the stress state at any point remains on the loading surface, and the flow rule $d\varepsilon_{ij}^{p} = d\lambda \frac{\partial g}{\partial \sigma_{ij}}$ (where $d\lambda$ is a scalar defining the plastic strain magnitude and g is the plastic potential function), the stress-strain incremental relationship Eq. (18) can be rewritten as follows:

$$d\sigma_{ij} = \left[C_{ijkl} - \frac{C_{ijmn}\frac{\partial f}{\partial \sigma_{qp}}\frac{\partial g}{\partial \sigma_{mn}}C_{qpkl}}{h + \frac{\partial f}{\partial \sigma_{rs}}C_{rstu}\frac{\partial g}{\partial \sigma_{tu}}} \right] d\varepsilon_{kl} \tag{19}$$

where $h = -\frac{1}{d\lambda}\frac{\partial f}{\partial k}d\kappa$ and κ is the hardening parameter (see Appendix I).

A return mapping algorithm (Ortiz and Simo 1986) has been used for solving the integration of the elasto-plastic constitutive relations of the current problem. For the current model, this algorithm includes the following steps:

(I) Geometric update (strain increments in the axial z direction):

$$\varepsilon_{z,\,n+1} = \varepsilon_{z,\,n} + d\varepsilon_z$$

(II) Solution of the elastic problem (elastic predictor):

$$\boldsymbol{\varepsilon}^{p(0)}_{n+1} = \boldsymbol{\varepsilon}^{p}_{n}$$

$$\boldsymbol{\varepsilon}^{e(0)}_{n+1} = \boldsymbol{\varepsilon}_{n+1} - \boldsymbol{\varepsilon}^{p(0)}_{n+1}$$

$$\kappa^{(0)}_{n+1} = \kappa_n \ (hardening) \quad \text{or} \quad \psi^{(0)}_{n+1} = \psi_n \ (softening)$$

$$\boldsymbol{\sigma}^{(0)}_{n+1} = \boldsymbol{\sigma}(\boldsymbol{\varepsilon}^{e(0)}_{n+1}, \boldsymbol{k}^{(0)}_{n+1}, \psi^{(0)}_{n+1})$$

(III) Check for "yielding" – is the concrete still within its elastic range?:

$$\text{if} \quad f^{(0)}_{n+1} \le 0$$

YES: $\boldsymbol{\varepsilon}^{p}_{n+1} = \boldsymbol{\varepsilon}^{p(0)}_{n+1}$; $\boldsymbol{\varepsilon}^{e}_{n+1} = \boldsymbol{\varepsilon}^{e(0)}_{n+1}$; $\boldsymbol{\sigma}_{n+1} = \boldsymbol{\sigma}^{0}_{n+1}$; $\kappa_{n+1} = \kappa^{(0)}_{n+1}$

GOTO (I) (Geometric update)

NO: $i = 0$

(IV) Plastic correctors:

$$\Delta\lambda = \frac{f^{(i)}_{n+1}}{f^{(i)}_{,\sigma(n+1)}\mathbf{C}g^{(i)}_{,\sigma(n+1)} - f^{(i)}_{,\kappa(n+1)}H^{(i)}_{n+1}}$$

$$\kappa^{(i+1)}_{(n+1)} = \kappa^{(i)}_{(n+1)} + \Delta\lambda H^{(i)}_{n+1}$$

$$\alpha^{(i+1)}_{(n+1)} = \alpha^{(i)}_{(n+1)} + \Delta\lambda L^{(i)}_{n+1}$$

$$\sigma^{(i+1)}_{n+1} = \sigma^{(i)}_{n+1} - \Delta\lambda C g^{(i)}_{,\sigma(n+1)} \Rightarrow f^{(i+1)}_{n+1}$$

where, $f_{,\sigma} = \frac{\partial f}{\partial \boldsymbol{\sigma}}, \quad g_{,\sigma} = \frac{\partial g}{\partial \boldsymbol{\sigma}}, \quad f_{,\kappa} = \frac{\partial f}{\partial \kappa}, \quad H = \frac{\partial \kappa}{\partial \varepsilon_p} d\varepsilon_p + \frac{\partial \kappa}{\partial \varepsilon_{p\max}} d\varepsilon_{p\max}$

$$L = \frac{\partial \alpha}{\partial \varepsilon_p} d\varepsilon_p + \frac{\partial \alpha}{\partial \varepsilon_{v\max}} d\varepsilon_{v\max}$$

(V) Check convergence: if $f_{n+1}^{(i+1)} \le TOLERANCE \left| f_{n+1}^{(0)} \right|$

NO: $i + 1 \rightarrow i$ GOTO (IV) (Plastic correctors)

YES: Check equilibrium at the concrete-steel boundary. This equilibrium condition corresponds to a compatibility condition, which requires equal tangential strains of the concrete and of the confining steel at the concrete-cylinder's perimeter. Force equilibrium of half a cylinder's cross-section (Fig. 6) yields the relation between the lateral pressure, p (or σ_{lat}) and the tension stress that develops in the equivalent steel f_s, which is a function of the tangential strain at the concrete-cylinder's perimeter (and of the steel's constitutive relations).

if $\sigma_{lat} = -f_s \cdot t_{eq1}$ (see Fig. 6)

NO: $\sigma_{lat} = -f_s \cdot t_{eq1}$ GOTO (II)

YES: $\boldsymbol{\sigma}_{n+1} = \boldsymbol{\sigma}_{n+1}^{(i+1)}; \quad \boldsymbol{\varepsilon}_{n+1}^{e} = \boldsymbol{\varepsilon}^{e}(\sigma_{n+1}, k_{n+1}); \quad \kappa_{n+1} = \kappa_{n+1}^{(i+1)}; \quad \boldsymbol{\varepsilon}_{n+1}^{p} = \boldsymbol{\varepsilon}_{n+1} - \boldsymbol{\varepsilon}_{n+1}^{e}$

GOTO (I) (Geometric update)

The simulation terminates when the plastic strain reaches its ultimate value ε_{pult} (see Appendix I), which indicates that the state of stress has reached the residual strength envelope. Note that in some cases this condition may result in from rupture of the lateral steel, which in this case determines the mode of failure (see also *section 4.7*).

Description and definition of the variables that are used in the above solution procedure are given in Appendix I. Note that bold parameters represent tensors and "(0)" and "(i)" superscripts denote initial and ith steps (respectively). Also note that when the concrete reaches a state of softening the parameter ψ (see Eq. (A.3) in Appendix I) is used instead of the hardening parameter κ.

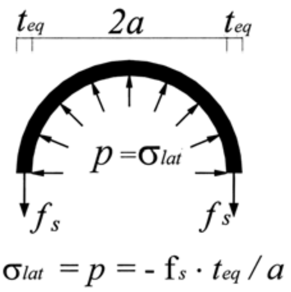

Fig. 6 Equilibrium at the concrete-steel boundary

4. Comparison with test results

Published test results (of the measured longitudinal stress and strain) of various RC columns are compared in Figs. 7-14 with their analytical simulations by the proposed model. The tests that were analyzed cover a relatively wide range of the problem's parameters (i.e., cylinder's diameter, that ranges from 145 to 500 mm, concrete strength that ranges from 25 to 72 MPa, steel yield strength

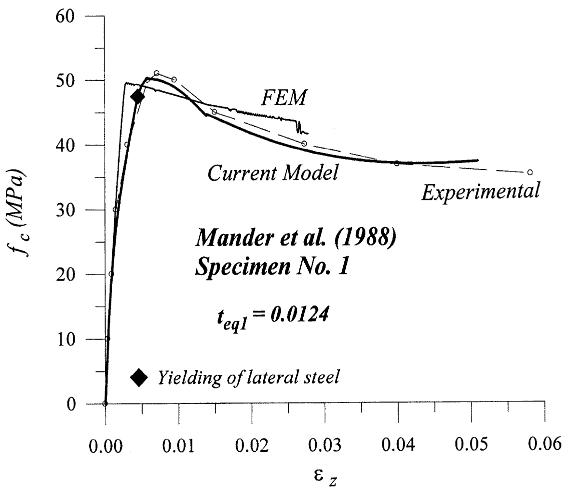

Fig. 7 Experimental and analytical axial behavior of *specimen No. 1* tested by Mander *et al.* (1988) (f_{c0} = 29 MPa, D = 500 mm, ϕ_t = 12 mm, $s_b = s + b$=41 mm, f_y = 340 MPa).

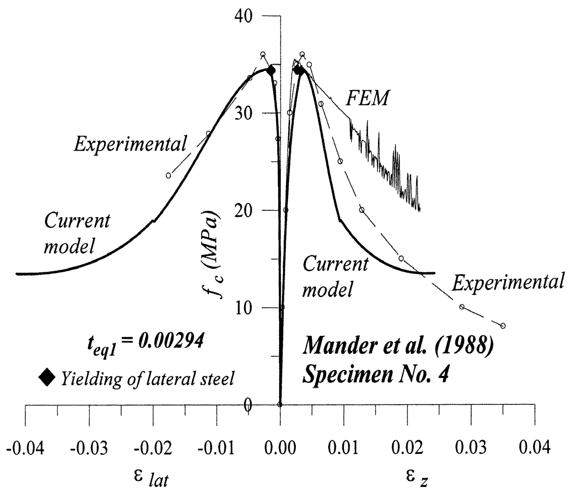

Fig. 8 Experimental and analytical axial and lateral behavior of *specimen No. 4* tested by Mander *et al.* (1988) (f_{c0} = 29 MPa, D = 500 mm, ϕ_t = 10 mm, $s_b = s + b$ = 119 mm, f_y = 320 MPa)

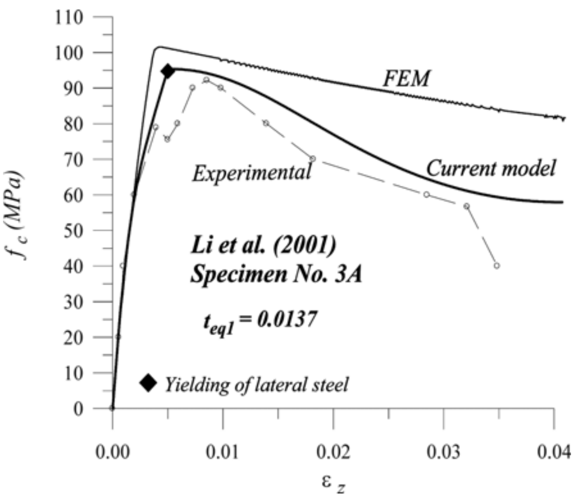

Fig. 9 Experimental and analytical axial behavior of *specimen 3A* tested by Li *et al.* (2001) (f_{c0} = 63 MPa, D = 240 mm, ϕ_t = 6 mm, $s_b = s + b$ = 20 mm, f_y = 445 MPa)

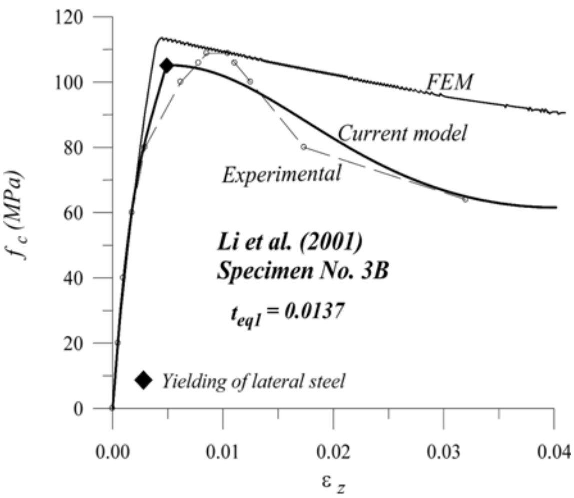

Fig. 10 Experimental and analytical axial behavior of *specimen 3B* tested by Li *et al.* (2001) (f_{c0} = 72.3 MPa, D = 240 mm, ϕ_t = 6 mm, $s_b = s + b$ = 20 mm, f_y = 445 MPa)

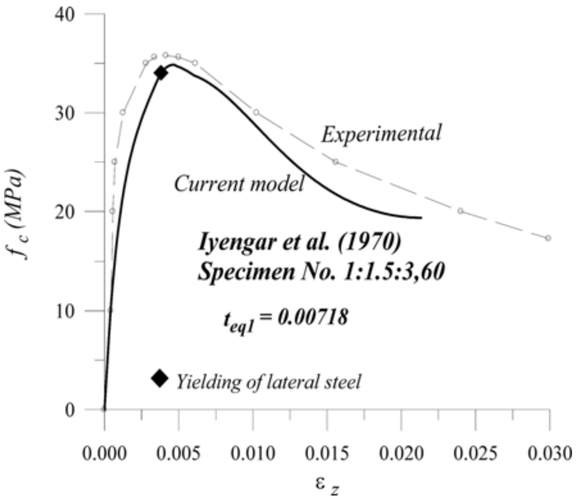

Fig. 11 Experimental and analytical axial behavior of *specimen 1:1.5:3,60* tested by Iyengar *et al.* (1970) (f_{c0} = 25.08 MPa, D = 150 mm, ϕ_t = 6.5 mm, $s_b = s + b$ = 60 mm, f_y = 318.7 MPa)

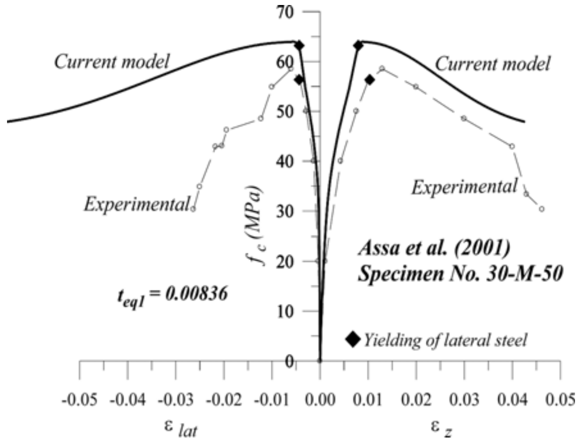

Fig. 12 Experimental and analytical axial and lateral behavior of *specimen 30-M-50* tested by Assa *et al.* (2001) (f_{c0} = 34.13 MPa, D = 145 mm, ϕ_t = 6.25 mm, $s_b = s + b$ = 50 mm, f_y = 909 MPa)

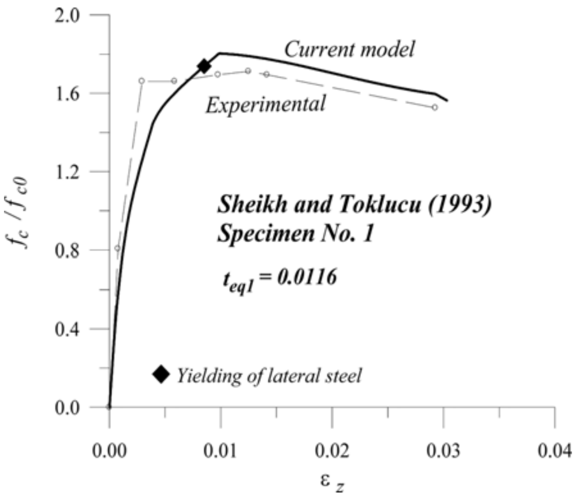

Fig. 13 Experimental and analytical axial behavior of *specimen No. 1* tested by Sheikh and Toklucu (1993) (f_{c0} = 35.9 MPa, D = 356 mm, ϕ_t = 11.3 mm, $s_b = s + b$ = 55.9 mm, f_y = 452 MPa)

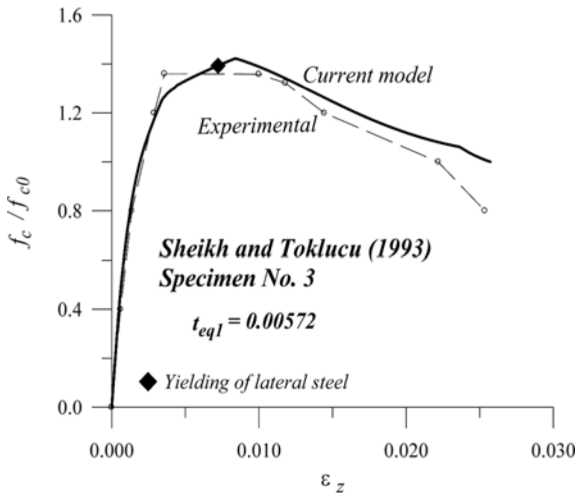

Fig. 14 Experimental and analytical axial behavior of *specimen No. 3* tested by Sheikh and Toklucu (1993) (f_{c0} = 35.9 MPa, D = 356 mm, ϕ_t = 11.3 mm, $s_b = s + b$ = 111.3 mm, f_y = 452 MPa)

that ranges from 320 to 900 MPa and tie spacing that ranges from 0.19 to 0.84 of the column radius), as detailed in Table 1.

Note that the expression of the thickness t_{eq} has been developed for confining rings with a rectangular cross-section whereas the ties' cross section is circular. Therefore, the width of the rings

Table 1 Geometrical and mechanical properties of tests that were simulated by the proposed model

Reference	Specimen No.	D mm	ϕ_t mm	$c^{(4)}$ mm	a mm	$s_b^{(3)}$ mm	s_1	b_1	$s_1 + b_1$	t_1	$m^{(1)}$ E_s/E_c	$t_1 m$	ρ_v (%)	f_{c0} MPa	$f_y^{(2)}$ MPa
Mander *et al.* (1988)	1	500	12	25	219	41	0.132	0.055	0.187	0.043	8.1	0.348	2.52	29	340 (EPH)
Mander *et al.* (1988)	4	500	10	25	220	119	0.495	0.045	0.54	0.036	8.1	0.288	0.60	29	320 (EPH)
Li *et al.* (2001)	3A	240	6	15	102	20	0.137	0.059	0.196	0.046	5.3	0.244	2.77	63	445 (EPP)
Li *et al*. (2001)	3B	240	6	15	102	20	0.137	0.059	0.196	0.046	4.9	0.228	2.77	72.3	445 (EPP)
Iyengar *et al.* (1970)	1:1.5:3,60	150	6.5	0	71.8	60	0.746	0.091	0.837	0.071	8.4	0.597	1.54	25.1	318.7 (EPP)
Assa *et al.* (2001)	30-M-50	145	6.25	0	69.375	50	0.631	0.090	0.721	0.071	7.2	0.509	1.77	34.13	909 (EPP)
Sheikh & Toklucu (1993)	1	356	11.3	22	150.15	55.9	0.297	0.075	0.372	0.059	7.0	0.414	2.39	35.9	452 (ML)
Sheikh & Toklucu (1993)	3	356	11.3	22	150.15	111.8	0.669	0.075	0.744	0.059	7.0	0.414	1.20	35.9	452 (ML)

(1) $E_s = 210000$ MPa, $E_c = 5000\sqrt{f_{c0}}$ (MPa).
(2) Steel constitutive relations; (EPP) = Elastic-perfectly plastic, (EPH) = Elastic-perfectly plastic with hardening, (ML) = Multi-linear (see Fig. 5).
(3) $s_b = s + b$.
(4) c = concrete cover.

Table 2 Comparison between test results and the proposed model

(1)	(2)	(3)	(4)	(5)	(6)	(7)	(8)	(9)	(10)	(11)
Reference	Specimen No.	Confined strength f_{cc} (MPa)			Confined strain ε_{cc}			Strain at $0.85 \cdot f_{cc}$ ε_{c85}		
		Experi-mental	Model	Experi-mental/ Model	Experi-mental	Model	Experi-mental/ Model	Experi-mental	Model	Experi-mental/ Model
Mander *et al.* (1988)	1	51	50.3	1.01	0.0073	0.006	1.22	0.0188	0.018	1.04
Mander *et al.* (1988)	4	36	34.53	1.04	0.0033	0.0034	0.97	0.0063	0.006	1.05
Li *et al.* (2001)	3A	92.2	95.45 [95.08]	0.97 [0.97]	0.0085	0.0053 [0.0076]	1.6 [1.12]	0.0153	0.0176 [0.0171]	0.87 [0.89]
Li *et al.* (2001)	3B	108.8	105.3 [104.8]	1.03 (1.04]	0.0085	0.005 [0.0074]	1.7 [1.15]	0.0142	0.0164 [0.0162]	0.87 [0.88]
Iyengar *et al.* (1970)	1:1.5:3,60	35.78	34.86	1.03	0.0041	0.0046	0.89	0.0099	0.0096	1.03
Assa *et al.* (2001)	30-M-50	58.18	63.99 [63.25]	0.91 [0.92]	0.0132	0.009 [0.0143]	1.46 [0.92]	0.032	0.0286 [0.0281]	1.12 [1.14]
Sheikh & Toklucu (1993)	1	61.03	64.74	0.94	0.0133	0.01	1.33	Not Available	Not Available	-
Sheikh & Toklucu (1993)	3	48.82	51.06	0.96	0.0068[(1)]	0.0084	0.81[(1)]	0.016	0.0163	0.98

[…] Multi-linear (ML in Fig. 5) stress-strain behavior of the steel.
(1) Average that corresponds to ε_{cc} ranging between 0.0036 and 0.01 (see also Fig. 14). Note that Sheikh & Toklucu (1993) used the lower value of 0.0036.

Table 2 Continued

(12)	(13)	(14)	(15)	(16)	(17)	(18)	(19)
Reference	Specimen No.	Lateral pressure at peak stress $\sigma_{lat,c}$ (MPa)			Ultimate axial strain ε_{cu}		
		Experimental	Model	Experimental/ Model	Experimental	Model	Experimental/ Model
Mander *et al.* (1988)	1	-	4.22	-	0.058	0.051	1.14
Mander *et al.* (1988)	4	$0.96^{(2)}$	0.94	1.02	0.035	0.024	1.46
Li *et al.* (2001)	3A	-	6.11	-	0.035	0.04	0.88
Li *et al.* (2001)	3B	-	6.11	-	0.032	0.041	0.78
Iyengar *et al.* (1970)	1:1.5:3,60	-	2.28	-	0.03	0.021	1.43
Assa *et al.* (2001)	30-M-50	$7.68^{(2*)}$	7.6 [7.6]	1.01 [1.01]	0.0462	$0.049^{(3)}$ $(0.043)^{(3)}$	$0.94^{(3)}$ $(1.07)^{(3)}$
Sheikh & Toklucu (1993)	1	$6.89^{(2*)}$	5.88	1.17	0.0293	0.038 (0.0304)	0.77 (0.96)
Sheikh & Toklucu (1993)	3	$2.71^{(2*)}$	2.95	0.92	0.0253	0.0277 (0.0258)	0.91 (0.98)

[…] Multi-linear (ML in Fig. 5) stress-strain behavior of the steel;
(…) failure is indicate by rupture of the steel ties (applicable with reported values of the steel's rupture strain).
(2) Calculated from the thin-tube analogy using the measured spiral strain values. (2*) Calculated by the reference authors.
(3) In this case the steel's multi-linear and the elastic-perfectly plastic (ML and EPP in Fig. 5, respectively) stress-strain behavior results in the same concrete ultimate axial strain.

in the analysis of reinforcing ties is taken as equal to the tie diameter ϕ_t (i.e., $b = \phi_t$) and the rings' thickness (t) is set to match the cross-section areas of the ring to that of the tie, i.e., $t = \frac{\pi}{4}b\left(= \frac{\pi}{4}\phi_t\right)$. It is also noted that the observation that there is no difference between the confinement provided by spirals and by hoops (Sheikh and Toklucu 1993) is applied in the current model.

In the following comparison of the model with test results of relatively large-scale specimens, both analytical and published experimental results refer to the confined core and they include neither the concrete cover nor the longitudinal steel (the effects of these parameters can be added to the response of the confined concrete core). However, for the small-scale specimens 1:1.5:3,60 and 30-M-50 (see in Table 1 Iyengar *et al.* 1970, Assa *et al.* 2001, respectively) the current analysis as well as the published experimental results refer to the full diameter of the specimens, which includes the effect of the concrete cover. In these cases the behavior of the concrete cover was modeled according to the unconfined concrete stress-strain curves published by Mander *et al.* (1988): it was taken into account as long as the axial strain (ε_z) was smaller or equal to the spalling strain (ε_{sp} = 0.006), where for ε_z that was larger than $2\varepsilon_{c0}$ (and smaller than ε_{sp}) the uniaxial stress-strain relationship of the cover was assumed to be a straight line which reaches zero stress at a strain equal to ε_{sp} (Mander *et al.* 1988). Note though, that in these small scale tests the thickness of concrete cover was equal to half of the diameter of the confining ties and no longitudinal reinforcement was used.

4.1 Overall response

Figs. 7-14 show that there is a good agreement between the overall response predicted by the model and the corresponding experimental results. In addition to the overall response Table 2 shows a comparison between the experimental and the analytical values of the confined concrete strength f_{cc}, of its corresponding axial strain ε_{cc}, the strain at 85% of the concrete strength, ε_{c85}, the lateral pressure at peak axial stress, $\sigma_{lat,cc}$, and the ultimate axial strain, ε_{cu}.

4.2 Confined strength, f_{cc}

Table 2 shows that the model's prediction of the confined strength is within −4% to +6% of the experimental measurements (column 5 in Table 2). It can be seen that the type of constitutive relations of the steel (elastic-perfectly plastic vs. multi linear) does not have an influence on this result.

4.3 Strain at peak stress, ε_{cc}

A somewhat lesser agreement between the model and the experimental results has been obtained for the strain ε_{cc} that corresponds to the confined strength (column 8 in Table 2). It is interesting to note that using a multi-linear stress-strain model for the steel (ML curve in Fig. 5) in the simulations of the tests reported by Assa *et al.* (2001), Li *et al.* (2001), significantly improved the model results: the analytical strains ε_{cc} of these cases, which were 46, 60 and 70 percent lower than their corresponding experimental values when the EPP material model (see Fig. 5) was used to simulate the steel, were only 8 percent higher, and 12 and 15 percent lower when the multi-linear relations (with f_{su} equal to f_y that was used for the EPP model) were used. The results that were obtained with the ML steel model are given in square brackets in column 8, Table 2. Note that the strength of the steel, which was used in these tests, was higher than 400 MPa (Table 1). It is likely that this type of steel has rounded stress-strain curves (e.g., Legeron and Paultre 2003). Therefore, the multi-linear (ML in Fig. 5) stress-strain curve may be more adequate to model this type of steel.

4.4 Strain at 85% of the concrete strength, ε_{c85}

Column 11 in Table 2 shows that there is a good agreement between the analytical and the experimental results that were measured of ε_{c85} (strain at 85% of the concrete strength). Similarly to the simulated values of the confining strength, the steel constitutive model did not have a significant influence on the analytical values of ε_{c85}. This is shown by the results of ε_{c85} that were obtained with the elastic-perfectly plastic versus the multi-linear models (values without brackets versus values in brackets, respectively, in columns 10 and 11, Table 2) for the lateral steel, which differed from each other by only 1-3% (columns 10 and 11, Table 2).

4.5 Lateral behavior

Figs. 8 and 12 show the axial and lateral response predicted by the model and the corresponding available experimental results. It can be seen in Fig. 8 that there is a good agreement between the predicted and the experimental results for specimen No. 4, tested by Mander *et al.* (1988). As for specimen No. 30-M-50 (tested by by Assa *et al.* 2001) - Fig. 12 shows that there is a good agreement between the predicted and the experimental results only at the pre-peak behavior. It is noted that this specimen had relatively small dimensions (145 × 300 mm) and high strength confining steel (with f_y = 909 MPa, Table 1), which may need a material model for its simulation that is different than that used in the current work.

The stress of the lateral steel, as predicted by the model, is indicated in Figs. 7-14, which together with Table 2 show that there is a fair to good agreement between the analytical and the experimental results of the lateral pressure at peak stress, $\sigma_{lat,cc}$ (col. 16 in Table 2).

4.6 Ultimate axial strain

Table 2 shows that there is a fair agreement between the analytical and the experimental results that were measured of the axial strain ε_{cu} (col. 19 in Table 2). It is worth noting that the best agreement between the model's prediction and the experimental results is achieved when the measured rupture strain of the steel is well defined (or known). As mentioned in section 3.3 the simulation terminates when the concrete plastic strain reaches its ultimate value ε_{pult} (see Appendix I), which indicates that the state of stress has reached the residual strength envelope. However, another indicator for terminating the simulation is when the lateral strain reaches the rupture strain of the confining steel (as explained in the following section).

4.7 Mode of failure

Usually for highly confined concrete columns the failure mode is rupture (or snapping) of the ties followed by concrete crushing (e.g., see Mander *et al.* 1988, Li *et al.* 2001) and for lowly confined concrete columns the failure mode is buckling of longitudinal bars, followed or accompanied by concrete crushing and rupture of the steel ties (with smaller angle of the failure plane measured from the vertical axis and strongly defined diagonal failure plane). Since the current model deals only with the confined concrete core it cannot simulate directly buckling of the longitudinal bars. Therefore, failure is indicated in the model by the concrete crushing (i.e., when $\varepsilon_p = \varepsilon_{pult}$) and if there is rupture of the ties – it is indicated as well.

Out of the cases that were checked (Table 1) the measured stress-strain behavior of the steel ties has been given only for three specimens (30-M-50 by Assa *et al.* 2001 and specimens 1 and 3 by Sheikh and Toklucu 1993). The corresponding calculated results that were obtained with the reported steel rupture strains of these tests differ only by 2 to 7% from the experimental results (see values given in brackets in col. 19, Table 2) and in these cases the authors reported rupture of the confining ties. This shows that using the measured rupture strain of the steel ties (rather than a "typical" stress-strain curve) gives better results for the ultimate axial strain. In four specimens (1 and 4 tested by Mander, 3A and 3B tested by Li *et al.*) a typical (i.e., not specific) stress-strain behavior of the steel was given and for these cases the analytical lateral strain at concrete crushing was less than the rupture strain. In these cases Mander *et al.* (1988) reported "hoop fracture with a strongly defined diagonal failure plane" in Column 4 and a failure that was due to the hoop fracture with a "lack of well defined failure mode for well-confined columns" (such as column 1). Li *et al.* (2001) reported that the failure observed for specimens confined by normal yield strength steel was "usually gradual and quite gentle after the first transverse bar fractured".

5. Finite element analysis

A numerical FEM analysis was carried out in order to compare the model results with those of the FEM analysis. Furthermore, distribution of the stresses and strains along a typical zone of the concrete cylinder at the stage of its plastic behavior, which can not be measured experimentally, can be examined and studied with this numerical tool. The ATENA 2D (2003) computer program was used to carry out the non-linear FEM simulations of four experiments whose details are given in the first four rows of Tables 1 and 2. These tests had volumetric steel tie ratios that ranged between 0.6 to 2.5 percent, as well as low and high values of their diameters, spacing and unconfined concrete strengths (Table 1).

5.1 FEM mesh and material models

The axisymmetrical cylinder has been modeled by isoparametric axisymmetric, 4-nodes quadrilateral and 3-nodes triangle elements. Each of the transverse ties is represented by six one-node axisymmetric circumferential truss element (Axisymmetric truss elements have been used in order to avoid shear stresses at the cylinder-ring boundary). A typical axi-symmetric model is shown in Eid (2004).

The concrete material model of the ATENA 2D FEM program uses the Menetrey and Willam (1995) failure surface, which is described in Appendix II. An elasto-plastic with hardening material law was used to simulate the steel. Its parameters were equal to those that were used in the current analytical model (see Fig. 5).

5.2 FEM results

Figs. 7-10 show the stress-strain curves of the experiments that were simulated by the FEM analysis. The use of different concrete material models for the FEM analysis and for the analytical model yielded stress-strain curves of the concrete columns, which had similar shapes with differences that were mainly in the post-peak range (Figs. 7-10). It is noted that the reasons for performing the FEM analysis were to examine the equivalency criterion and the stress and strain distributions in the confined concrete along a typical zone at the concrete plastic range. Therefore, although the axial post peak behaviour of the model and of the FEM are not the same, the use of the FEM analysis is appropriate and important for the above reasons, i.e., examination and study of the concrete stress and strain distributions and of stresses and strains that develop at the lateral steel reinforcement (including at the stage of the concrete plastic behavior). Thus, the results of the FEM analysis support the equivalency criterion of the proposed model. This is demonstrated in Figs. 15 and 16, which show (respectively) the lateral steel stress (vs. the concrete axial strain ε_z) and the

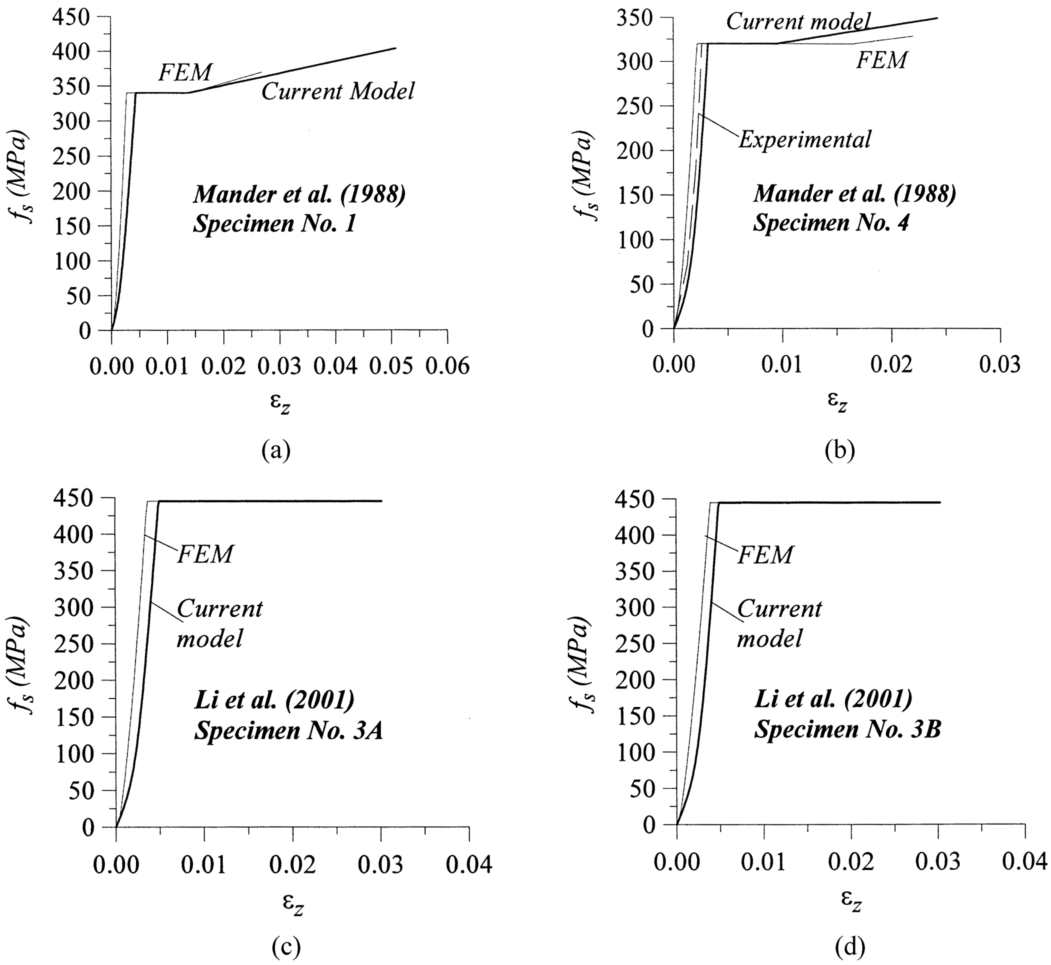

Fig. 15 FEM and analytical results of the circumferential steel stress versus axial strain ε_z

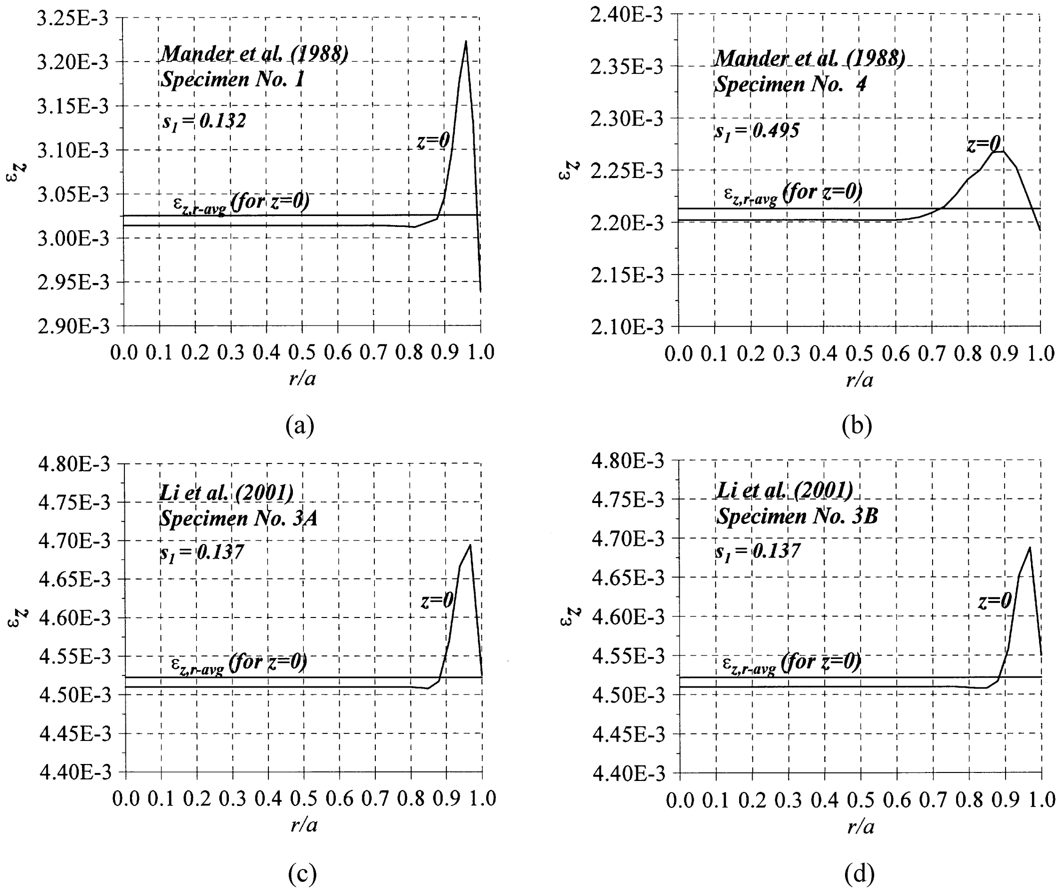

Fig. 16 FEM calculations of the axial strain distribution along the radius for $z = 0$ at concrete peak stress

radial distribution of the axial strain (at $z = 0$) at the stage of the concrete plastic response (at peak stress). Fig. 15 shows a good agreement between the results of the proposed model, of the tests (specimen 4) and of the FEM analysis.

Fig. 16 shows that similarly to the elastic behavior, the axial strain distribution is constant within a reduced cylinder radius also when the concrete behavior is plastic. It can be seen in the figure that when the axial strain is averaged along the cylinder radius ($\varepsilon_{z,\,r\text{-}avg}$ in Fig. 16) the value of the constant strain is very close to that of $\varepsilon_{z,\,r\text{-}avg}$. Furthermore, this result is hardly influenced by the ties spacing: the difference between $\varepsilon_{z,\,r\text{-}avg}$ and the constant value of ε_z is less than 0.5% for s_1 values of 0.13, 0.14 or 0.5 (Figs. 16(a), 16(c,d) and 16(b), respectively). These results indicate that the equivalency criterion (see *section 2.2*), which is set at the stage of the elastic response, holds in the plastic range as well.

6. Influence of the problem's variables on the confinement

According to the proposed model, the efficiency of the lateral reinforcement can be evaluated

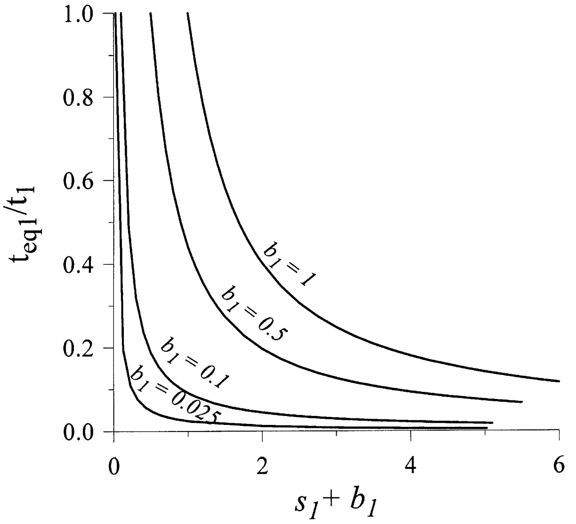

Fig. 17 t_{eq1}/t_1 versus steel tie spacing $s_1 + b_1$ for different values of b_1, $t_1m = 0.7$ and $\nu = 0.2$

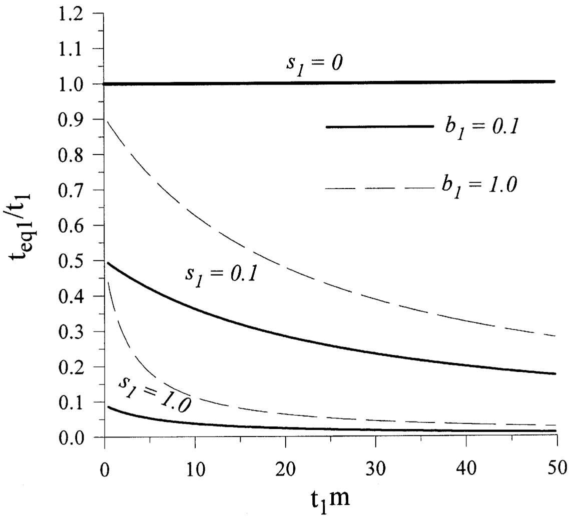

Fig. 18 t_{eq1}/t_1 versus t_1m for different values of s_1 and b_1, and for $\nu = 0.2$

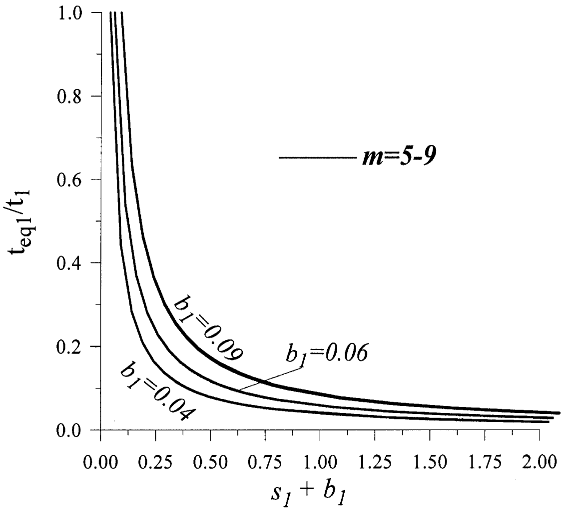

Fig. 19 t_{eq1} versus s_{b1} ($s_1 + b_1$) for reinforced concrete practical values of b_1, m and for $\nu = 0.15$

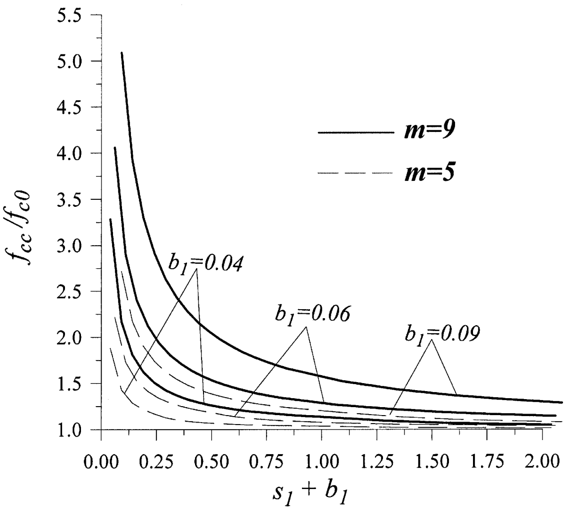

Fig. 20 Concrete strength enhancement versus tie spacing s_{b1} ($= s_1 + b_1$) and diameter for $f_y = 400$ MPa and for $m = 9$ and $m = 5$

according to the thickness t_{eq}: the thicker t_{eq} the higher the confinement effect. Figs. 17 and 18 show the effect of the different problem's variables on the normalized equivalent thickness t_{eq1}. These figures show that increasing the (normalized) ties spacing, $s_1 + b_1$ (Fig. 17), and t_1m (Fig. 18), results in a decrease of t_{eq1}/t_1, while increasing the (normalized) diameter of the steel cross-section, b_1, results in an increase of t_{eq1}/t_1. These figures also show that the current model converges well to the simple solution of zero tie spacing ($s_1 = 0$), where the equivalent thickness, t_{eq}, is equal to that of the ring thickness, t (t_{eq1}/t_1 = 1).

For practical cases of reinforced concrete the modules ratio m ranges from 5 to 9 and b_1 ranges from 0.04 to 0.09. Fig. 19 shows that in this range t_{eq1} depends only on the spacing $s_1 + b_1$ and on the ties diameter b_1. It is interesting to note that according to the proposed model and for practical cases of reinforced concrete, the equivalent uniform steel tube's thickness for a normalized spacing $s_1 + b_1$ that is larger than 0.5, is less than 0.15 of the reinforcing ties' diameter (recalling that in the current model $\phi_t = b = 4/\pi \cdot t$, where ϕ_t is the tie's diameter).

Fig. 20 demonstrates the influence of the normalized ties spacing, $s_1 + b_1$, and of the normalized tie diameter, b_1, on the confined strength f_{cc}, for f_y = 400 MPa (elastic-perfectly plastic steel behavior) and for m = 5 and m = 9 (which respectively correspond to concrete with unconfined strengths of 71 and 22 MPa). It can be seen that the effect of the confinement on enhancing the concrete strength is more pronounced for normal strength concrete than for higher strength concrete (compare in Fig. 20 solid and dashed lines that correspond to m = 9 and m = 5, respectively). The figure shows that the enhancement of the concrete confined strength is most significant within a tie spacing of up to about 0.5 of the column's radius ($s_1 + b_1 < 0.5$). Within this range the confined-to-unconfined concrete strength ratio can be as high as 5 and 2.75 for normal strength concrete (i.e. m = 9) and for higher strength concrete (i.e., m = 5), respectively. If, however, the spacing $s_1 + b_1$ is larger than 0.5 the strength enhancement is not greater than 2.0 (see m = 9 and b_1 = 0.09 in Fig. 20) and for most cases it is even smaller than 1.5.

7. Conclusions

This paper presents a theoretical model for the behavior of partially confined axi-symmetric reinforced concrete members subjected to axial load. The analysis uses the theories of elasticity and plasticity to cover the full range of the concrete behavior. This is done by replacing the incremental steel ties with an equivalent tube of thickness t_{eq} and by analyzing the concrete cylinder, which is uniformly confined by the equivalent tube. The diameter of the concrete cylinder is equal to that of the original problem (i.e., the diameter of the concrete core confined by the ties). The equivalency criterion initiates from a theoretical analysis of the problem in its elastic range where further finite element analysis shows that this criterion is valid also in the plastic range of the cylinder material. Comparisons with published test results of confined reinforced concrete stress-strain curves show good agreement between the analytical results and the test. However, these comparisons also showed that the calculation of the confined strain and the mode of failure (i.e., rupture of the confining reinforcement) is sensitive to the stress-strain behavior of the lateral steel.

The current model has three main limitations: It applies to unconfined concrete strengths of 28-73 MPa, according to the constitutive concrete model that was used in the analysis (Imran and Pantazopoulou 2001). It refers to the behavior of a typical zone in a RC column (and does not simulate phenomena that might occur at the ends of the column). Additionally, this model deals with the confined concrete core and it includes neither the longitudinal steel nor the concrete cover (whose response can be added separately). Therefore the current model cannot simulate directly the possibility of longitudinal bars buckling.

According to the proposed model, the efficiency of the lateral reinforcement can be evaluated by the thickness t_{eq}. It is shown that for practical cases of reinforced concrete the equivalent uniform steel tube's thickness for a normalized spacing $s_1 + b_1$ that is larger than 0.5, is less than 0.15 of the reinforcing ties' diameter. The model also shows that the effect of the confinement on enhancing the concrete strength is more pronounced for normal strength concrete than for higher strength concrete and that this effect is most significant up to a tie spacing of 0.5 of the column's radius. Within this range and for reinforcing ties with $f_y = 400$ MPa the confined-to-unconfined concrete strength ratio can be as high as 5 and 2.75 for normal strength concrete (i.e. $m = 9, f_{c0} \approx 22$ MPa) and for higher strength concrete (i.e., $m = 5, f_{c0} \approx 71$ MPa), respectively. When the spacing $s_1 + b_1$ is larger than 0.5 the strength enhancement is not greater than 2.0 and for most cases it is even smaller than 1.5.

Acknowledgements

This study was partially supported by the Israeli Ministry of Construction and housing.

References

Assa, B., Nishiyama, M. and Watanabe, F. (2001), "New approach for modeling confined concrete. I: Circular column", *J. Struct. Eng.,* ASCE, **127**(7), 743-757.

ATENA 2D (2003), Computer Program for Nonlinear Finite Element Analysis of Reinforced Concrete Structures, Cervenka Consulting, Version 2.1.

Cusson, D. and Paultre, P. (1995), "Stress-strain model for confined high-strength concrete", *J. Struct. Eng.,* ASCE, **121**(3), 468-477.

Eid, R. (2004), "Structural analysis of partially confined reinforced concrete in members with axi-symmetric cross-section and loading", Ph.D. Thesis, Department of Civil and Environmental Engineering, Technion-Israel Institute of Technology, Haifa, Israel.

Fafitis, A. and Shah, S.P. (1985), "Predictions of ultimate behavior of confined columns subjected to large deformations", *ACI Struct. J.*, **82**(4), 423-433.

Grassl, P., Lundgren, K. and Gylltoft, K. (2002), "Concrete in compression: A plasticity theory with a novel hardening law", *Int. J. Solids Struct.*, **39**, 5205-5223.

Hoshikuma, J., Kawashima, K., Nagaya, K. and Taylor, A.W. (1997), "Stress-strain model for confined reinforced concrete in bridge piers", *J. Struct. Eng.,* ASCE, **123**(5), 624-633.

Imran, I. (1994), "Applications of non-associated plasticity in modeling the mechanical response of concrete", Ph.D. Thesis, Dept. of Civil Engineering, University of Toronto, Toronto, ON, Canada.

Imran, I. and Pantazopoulou, S.J. (1996), "Experimental study of plain concrete under triaxial stress", *ACI Materials J.*, **93**(6), 589-601.

Imran, I. and Pantazopoulou, S.J. (2001), "Plasticity model for concrete under triaxial compression", *J. Eng. Mech.,* ASCE, **127**(3), 281-290.

Iyengar, K.T., Sundara, Raja, Desayi, P. and Reddy, K.N. (1970), "Stress-strain characteristics of concrete confined in steel binders", *Magazine of Concrete Research*, **22**(72), 173-184.

Karabinis, A.I. and Kiousis, P.D. (1994), "Effects of confinement on concrete columns: Plasticity approach", *J. Struct. Eng.,* ASCE, **120**(9), 2747-2767.

Legeron, F. and Paultre, P. (2003), "Uniaxial confinement model for normal- and high-strength concrete columns", *J. Struct. Eng.,* ASCE, **129**(2), 241-252.

Li, B., Park, R. and Tanaka, H. (2001), "Stress-strain behavior of high-strength concrete confined by ultra-high and normal-strength transverse reinforcement", *ACI Struct. J.*, **98**(3), 395-406.

Mander, J.B., Priestley, M.J.N. and Park, R.J.T. (1984), "Seismic design of bridge piers", Research Report No. 84-2, Univ. of Canterbury, New Zealand.

Mander, J.B., Priestley, M.J.N. and Park, R.J.T. (1988), "Theoretical stress-strain model for confined concrete", *J. Struct. Eng.,* ASCE, **114**(8), 1804-1826.

Mander, J.B., Priestley, M.J.N. and Park, R.J.T. (1988), "Observed stress-strain behavior of confined concrete", *J.*

Struct. Eng., ASCE, **114**(8), 1827-1849.
Menetrey, P. and Willam, K.J. (1995), "Triaxial failure criterion for concrete and its generalization", *ACI Struct. J.*, **92**(3), 311-318.
Ortiz, M. and Simo, J.C. (1986), "An analysis of a new class of integration algorithms for elastoplastic constitutive relations", *Int. J. Num. Methods in Eng.*, **23**, 353-366.
Park, R., Priestly, M.J.N. and Gill, W.D. (1982), "Ductility of square-confined concrete columns", *J. Struct. Eng.,* ASCE, **108**(4), 929-950.
Popovics, S. (1973), "A numerical approach to the complete stress-strain curves for concrete", *Cement and Concrete Research*, **3**(5), 583-599.
Richart, F.E., Brandtzaeg, A. and Brown, R.L. (1928), "The failure of plain and spirally reinforced concrete in compression", Bulletin No. 190, Engineering Experiment Station, University of Illinois, Urbana.
Saatcioglu, M. and Razvi, S.R. (1999), "Confinement model for high-strength concrete", *J. Struct. Eng.,* ASCE, **125**(3), 281-289.
Sheikh, S.A. and Uzumeri, S.M. (1980), "Strength and ductility of tied concrete columns", *J. Struct. Eng.,* ASCE, **106**(5), 1079-1102.
Sheikh, S.A. and Uzumeri, S.M. (1982), "Analytical model for concrete confinement in tied columns", *J. Struct. Eng.,* ASCE, **108**(12), 2703-2722.
Sheikh, S.A. and Toklucu, M.T. (1993), "Reinforced concrete columns confined by circular spirals and hoops", *ACI Struct. J.*, **90**(5), 542-553.
Scott, B.D., Park, R. and Priestly, M.J.N. (1982), "Stress-strain behavior of concrete confined by overlapping hoops at high and low strain rates", *J. Struct. Eng.,* ASCE, **79**(1), 13-27.

Appendix I

The functions of the hardening, failure and softening surfaces (respectively, f_{hard}, f_{fail}, f_{soft}) of the concrete material model (Imran and Pantazopoulou 2001) have the form of the Hsieh *et al.* (1988) function and they are given by the following expressions:

$$f_{hard} = A\frac{J_2}{\kappa f_{c0}} + B\sqrt{J_2} + C\kappa\sigma_1 + D\kappa I_1 + E_{htc}\frac{1-\kappa}{\kappa f_{c0}}I_1^2 - \kappa f_{c0} = 0 \tag{A.1}$$

$$f_{fail} = A\frac{J_2}{f_{c0}} + B\sqrt{J_2} + C\sigma_1 + DI_1 - f_{c0} = 0 \tag{A.2}$$

$$f_{soft} = A\frac{J_2}{f_{c0}} + B\sqrt{J_2} + C\sigma_1 + DI_1 - (I-\psi)\frac{I_1}{I_1^{trans}}f_{c0} - \psi f_{c0} = 0 \tag{A.3}$$

where f_{c0} is the uniaxial compressive strength of concrete and σ_1 is the major principal stress. The parameters A, B, C, D, E_{htc} are constants and I_1^{trans} is an empirically obtained function that depends on the concrete uniaxial compressive strength f_{c0} and represents the effect of the concrete physical properties on its strength characteristics (Imran and Pantazopoulou 2001). The hardening parameter, κ, ranges from κ_0 (= 0.37) at the initial hardening surface, when plasticity commences, to κ = 1.0, when the state of stress reaches the failure surface (Eq. A.1 becomes Eq. A.2). κ is defined by the following expression (Imran and Pantazopoulou 2001):

$$\kappa(\varepsilon_p, \varepsilon_{p\max}) = \frac{2\sqrt{\varepsilon_p\varepsilon_{p\max}} - \varepsilon_p}{\varepsilon_{p\max}}(1-\kappa_0) + \kappa_0 \tag{A.4}$$

where ε_p is the accumulated plastic strain:

$$\varepsilon_p = \int d\varepsilon_p = \int\frac{\sigma_{ij}d\varepsilon_{ij}^p}{\kappa f_{c0}} \tag{A.5}$$

and $\varepsilon_{p\max}$ is the value of the plastic strain when the state of stress reaches the failure surface:

$$\varepsilon_{p\max} = G_h(\varepsilon_{v\max} - \varepsilon^u_{v,\max}) + \varepsilon^u_{p\max} \tag{A.6}$$

where G_h is a material constant and $\varepsilon_{v,\max}$ is the maximum volumetric contraction experienced by the material. The superscript "u" denotes the strain data from uniaxial compressive tests. For cases of active confinement, in which the lateral pressure is constant during the increase of the axial strain, the maximum (contraction) volumetric strain $\varepsilon_{v,\max}$ can be determined empirically (Imran and Pantazopoulou 2001). However, for a concrete cylinder in which the lateral pressure is passive (such as the lateral pressure that develops by the steel ties) the maximum (contraction) volumetric strain increases with the increase of the lateral pressure. Therefore, a constant value of $\varepsilon_{v,\max}$ is not suitable for the case of passive confinement. In cases of axi-symmetric state of stress, $\varepsilon_{v,\max}$ can be calculated from the following expression, which was also proposed by Imran and Pantazopoulou (1996):

$$\varepsilon_v = (1-2\nu)\left[\frac{2\sigma_{lat}}{E_c} + \varepsilon_z^0\left(\frac{\varepsilon_z}{\varepsilon_z^0} - \left[\frac{\varepsilon_z - \varepsilon_z^{\lim}}{\varepsilon_z^0 - \varepsilon_z^{\lim}}\right]^2\right)\right] \tag{A.7}$$

where σ_{lat} is the lateral (radial) stress, ε_z is the axial strain, ε_z^0 is the axial strain at zero volumetric strain (taken as equal to the axial compressive strain at peak stress when softening commences) and $\varepsilon_z^{\lim}$ is the axial strain at which cracking occurs in the lateral direction.

The softening parameter, ψ (Eq. A.3), ranges from $\psi = 1.0$ at peak stress (Eq. A.3 becomes Eq. A.2) to $\psi = 0$ at the residual strength envelope. The parameter ψ is defined by the following expression (Imran and Pantazopoulou 2001):

$$\psi(\varepsilon_p, \varepsilon_{p\max}) = \frac{1}{2} + \frac{1}{2}\cos\left(\pi\frac{\varepsilon_p/\varepsilon_{p\max} - 1}{\varepsilon_{pult}/\varepsilon_{p\max} - 1}\right) \tag{A.8}$$

where ε_{pult} is the ultimate plastic strain at which the state of stress reaches the residual strength envelope (and the simulation terminates). It is given by the following expression:

$$\varepsilon_{pult} = 8.1\,\varepsilon_{p\max}(f_{c0}/30)^{0.95} \tag{A.9}$$

Plastic potential function

A Druker-Prager type criterion is used as the plastic potential function g for the non-associated plastic flow (see e.g., Karabinis and Kiousis 1994). The function g is given by:

$$g = \alpha\frac{I_1}{\sqrt{3}} + \sqrt{2J_2} - c = 0 \tag{A.10}$$

where c is a constant and α is the slope of the Druker-Prager function, which is evaluated based on test results as follows (Imran and Pantazopoulou 2001):

$$\alpha = \frac{\alpha_u}{(1-\eta)(\varepsilon_{v\max}/\varepsilon^u_{v\max})^{1/3}}\left(\frac{\varepsilon_p}{\varepsilon_{p\max}} - \eta\right) \tag{A.11}$$

where α_u is the value of a when uniaxially loaded concrete reaches its peak stress and η is the ratio $\varepsilon_p/\varepsilon_{p\max}$ at zero volumetric plastic strain under uniaxial compression, taken as 0.34 (Imran and Pantazopoulou 2001).

Appendix II

The concrete material which is used by ATENA 2D (2003) is given by the Menetrey and Willam (1995) failure surface F and the plastic potential g as follows:

$$F = \left[\sqrt{1.5}\frac{\rho}{f_{c0}}\right]^2 + m\left[\frac{\rho}{\sqrt{6}f_{c0}}r(\theta, e) + \frac{\xi}{\sqrt{3}f_{c0}}\right] - c = 0 \quad \text{(A.12)}$$

$$g = \beta_1\frac{1}{\sqrt{3}}I_1 + \sqrt{2J_2} \quad \text{(A.13)}$$

where,

$$r(\theta, e) = \frac{4(1-e^2)\cos^2\theta + (2e-1)^2}{2(1-e^2)\cos\theta + (2e-1)[4(1-e^2)\cos^2\theta + 5e^2 - 4e]^{1/2}} \quad \text{(A.14)}$$

$$m = \sqrt{3}\frac{f_{c0}^2 - f_t^2}{f_{c0}f_t}\frac{e}{e+1} \quad \text{(A.15)}$$

$$\xi = \frac{1}{\sqrt{3}}I_1; \quad \rho = \sqrt{2J_2}; \quad \cos 3\theta = \frac{3\sqrt{3}}{2}\frac{J_3}{J_2^{3/2}} \quad \text{(A.16)}$$

c is a hardening/softening parameter, which depends on the plastic strain and β_1 is a constant parameter.

Notation

a	: cylinder radius;
b	: width of lateral pressure band or ring;
C_{ijkl}	: isotropic material tensor
D	: gross diameter of RC column
E_c	: cylinder elastic modulus;
E_s	: elastic modulus of the reinforcement;
f_{c0}	: uniaxial concrete compressive strength;
f_{cc}	: confined concrete compressive strength;
f_y	: ring yield stress;
f_{hard}, f_{fail}, f_{soft}	: functions of the hardening, failure and softening surfaces;
g	: plastic potential function;
m	: confinement-to-cylinder modulus ratio, E_s/E_c;
I_1	: first invariant of the stress tensor;
J_2	: second invariant of the deviatoric stress tensor;
J_3	: third invariant of the deviatoric stress tensor;
k	: wave number;
p	: lateral pressure;
q	: axial pressure;
s	: ties spacing;
s_b	: center to center ties spacing;
t	: ring thickness;
t_{eq}	: ties equivalent thickness;
u	: radial displacement;
w	: axial displacement;
ε_{cu}	: ultimate axial strain;
ε_p	: accumulated plastic strain
ε_s	: tension strain of the confining reinforcement;
ε_{sp}	: concrete cover spalling strain;

ε_y : ring yield strain;
ε_z : axial strain;
ε_z^c : axial strain due to the action of the confining rings;
$\varepsilon_{z,r-avg}^c$: axial strain averaged over the radius at a given z due to the action of the rings;
$\varepsilon_{z,avg}^c$: axial strain due to action of the rings, averaged over the radius and over z, within a typical zone;
$\varepsilon_{z,avg}$: total axial strain averaged over the radius and over z within a typical zone;
$\varepsilon_{z,tu}$: axial strain in the equivalent tube;
ε_{cc} : confined concrete compressive strain;
ε_{c85} : strain at 85% of the concrete strength;
ε_{ij}, $\boldsymbol{\varepsilon}$: strain tensor;
ϕ_t : diameter of reinforcing ties;
κ : hardening parameter;
$\sigma_{lat} = p$: lateral pressure;
$\sigma_{lat,cc}$: lateral pressure at peak axial stress;
σ_{ij}, $\boldsymbol{\sigma}$: stress tensor;
ν : Poisson's ratio;
ψ : softening parameter;

Dimensionless variables:
b_1 : b/a;
k_1 : ka;
r_1 : r/a;
s_1 : s/a;
t_1 : t/a;
t_{eq1} : t_{eq}/a;